Experimental and Analytical Study of Contact Melting in a Rectangular Cavity

Z. F. Dong,* Z. Q. Chen,† Q. J. Wang‡
Xi'an Jiaotong University, Xi'an, People's Republic of China
and
M. A. Ebadian§
Florida International University, Miami, Florida 33199

This paper reports on a detailed investigation of analytical and experimental findings for contact melting in a rectangular cavity with phase change materials (PCM) of *n*-heptadecane and *n*-eicosane (research grade purity). Specifically, consideration is given to the rectangular cavity with inside dimensions of 100 × 60 × 50 mm. The temperature of the two side walls and bottom surface of the cavity are maintained constant by circulating water through a highly sensitive thermostat. The other surfaces are subjected to adiabatic conditions. The time-dependent solid-liquid interface contour is measured photographically during the melting process. According to the shadowgraph technique, the maximum displacement on the screen represents the temperature gradient. This temperature gradient on the wall is measured by the shadowgraph method, which results in calculation of the local Nusselt number. This local Nusselt number is used to show the difference between contact melting and fixed melting in the rectangular cavity at the same boundary conditions. Based on observation of the melting phenomena and data obtained, a theoretical model is developed and its solution is derived analytically. For the purpose of data reduction, a scale analysis method is used to find the functional dependence of the dimensionless parameters. The theoretical prediction is compared with experimental data and an excellent agreement is obtained. It is concluded that heat conduction in the melting phase is the controlling effect in the rectangular cavity.

Nomenclature

Ar = Archimedes number, $Ar = (\rho_s - \rho_\ell)/\rho_\ell\, gL^3/\nu^2$
C = specific heat, J kg^{-1} K^{-1}
Fo = Fourier number, $Fo = \alpha_\ell t/L^2$
g = gravity, m s^{-2}
h = local heat transfer coefficient, W m^{-2} K^{-1}
h_m = latent heat-of-fusion, J kg^{-1}
h_m^* = modified latent heat-of-fusion, Eq. (7)
H = instantaneous height of solid, m
H^* = dimensionless height of solid, $H^* = H/L$
k = thermal conductivity, W m^{-1} K^{-1}
L = characteristic length, m, $L = W$ in the modeling and $L = \bar{x}$ in the scale analysis
M = factor defined by Eq. (11)
Nu = local Nusselt number, $Nu = hz/k_\ell$
Pr = Prandtl number, $Pr = \mu C_\ell/K$
Sc = subcooling parameter, $Sc = C_s(T_m - T_o)/h_m$
Ste = Stefan number, $Ste = C_\ell(T_w - T_m)/h_m$
Ste^* = modified Stefan number, $Ste/(1 + Sc)$
t = time, s
T = temperature, K
u, v = velocities in x and z directions, m s^{-1}
$\bar{U}$ = dimensional decending velocity of solid PCM, m s^{-1}
$\bar{U}^*$ = dimensionless descending velocity of solid
V = volume of melted liquid, m^3
V_o = total volume of liquid PCM, m^3
V^* = dimensionless melting rate, $V^* = V/V_o$
W = width of the rectangular cavity, m
x, y, z = coordinates
$\bar{x}$ = instantaneous width of solid, $\bar{x} = W - 2\delta_1$, m
α = thermal diffusivity, m^2 s^{-1}
α^* = aspect ratio of solid PCM in initial state, $\alpha^* = H_o/W$
δ = dimensional melting layer thickness at the bottom, m
δ_1 = melting layer thickness on the vertical wall, m
δ_1^* = dimensionless melting layer thickness on vertical wall, δ_1/L
Δ = dimensionless melting layer thickness at the bottom, δ/L
λ = coefficient defined by Eq. (13)
μ = dynamic viscosity, kg m^{-1} s^{-1}
ρ = density, kg m^{-3}
ρ^* = solid-liquid density ratio, $\rho^* = \rho_s/\rho_\ell$
θ = temperature difference for PCM, K
ν = kinematic viscosity, $\nu = \mu/\rho$, m^2 s^{-1}

Subscripts
ℓ = liquid phase
s = solid phase
m = melting
o = initial state
w = wall

Received March 9, 1990; revision received June 8, 1990; accepted for publication June 12, 1990.

*Research Associate, Department of Mechanical Engineering; currently at Florida International University.
†Professor, Department of Power Machinery Engineering.
‡Associate Professor, Department of Power Machinery Engineering.
§Professor, Department of Mechanical Engineering.

Introduction

IT is widely recognized that solid-liquid phase change phenomena (melting and solidification) exist in many engineering applications, such as casting, welding, thermal control of spacecraft, nuclear reactor safety analysis, crystal growth, and thermal energy storage. In fact, inspection of literature surveys by Eckert,[1-3] Kakac,[4] Shah and London,[5] Soloukhin and Martynenko,[6] Martynenko,[7] Habib and Dallman,[8] and Viskanta[9,10] reveals that solid-liquid phase change material

has received significant attention in recent years. This, of course, is evident by the numerous publications in the open literature.

There are two kinds of melting phenomena: fixed melting and contact melting. When fixed melting occurs, the solid phase change material is forced to remain stationary and the melted liquid takes up the space between the solid-liquid interface and the heat source surface. On the other hand, in contact melting, the solid phase change material, or heat source, is free to move, or forced to move. Therefore, a microchannel exists between the solid-liquid interface and the heat source surface, and the melted liquid is forced to flow out of this channel. Accordingly, the study of contact melting is much more complicated than fixed melting. Investigations on contact melting for different geometries were performed and reported by several scientists experimentally, as well as theoretically. Among those, Emerman and Turcotte[11] reported on spherical geometry using Stokes' problem with melting. Moallemi and Viskanta[12,13] and Moallemi et al.,[14] reported on an experimental and analytical study of close contact melting for circular and rectangular cross sections. In their work, experiments were performed by placing a solid block on a horizontal planar heat source maintained at a constant surface temperature. Saito et al.[15–17] studied analytically/experimentally contact heat transfer with melting for cylindrical geometry. Analytical studies for tube geometry were performed by Saito et al.,[18] Bareiss and Beer,[19] Riviere and Beer,[20] Sparrow and Myrum,[21] and Sparrow and Geiger.[22] An analytical study of solidification and melting heat transfer to an unfixed phase change material inside a horizontal tube is reported by Betzel and Beer.[23] The study of contact melting in a rectangular cavity is completed by Dong.[24]

The main focus of this study is to report the experimental findings for contact melting in a rectangular cavity, and to present a complete theoretical model based on these experimental results. The temperature in this experiment is kept constant in two vertical walls and the bottom of the cavity; the other walls are subjected to adiabatic conditions. The time-dependent solid-liquid interface contour is measured photographically during the melting process. According to the shadowgraph technique, when a parallel light beam travels through the liquid phase, it will refract due to nonuniformity of the temperature gradient in the liquid. This temperature gradient is maximum on the heat source surface. Thus, the light beam near the surface will have a maximum refraction and a maximum displacement on the screen.[25] This maximum displacement represents the temperature gradient on the wall. This temperature gradient is measured by the shadowgraph method, which results in the calculation of local Nusselt number. For data reduction, the scale analysis method is applied to find the dependence relationship of the dimensionless parameters related to the contact melting in the rectangular cavity. Finally, the theoretical prediction from the model is developed in this paper and compared with experimental data, and an excellent agreement is obtained. For the geometry considered, it is observed that heat conduction is the dominant mechanism in contact melting.

It is believed that the availability of this solution is important for the design of heat storage element and potential application of electronic package cooling. This solution will, in turn, lead to a better understanding of contact melting, as well as fixed melting in a rectangular cavity.

Experimental Design

In this investigation, as shown in Fig. 1, the experimental system consists of eleven components. The beam from the He-Ne laser tube at section (1) travels through a pin hole (2), condenser (3), then it is reflected by two mirrors located at sections (4) and (5), and eventually forms a parallel beam. This beam passes through the test section (6) by properly aligning the mirrors (4) and (5). The shadowgraph on the screen (7) is measured by using a Nikon® camera at section

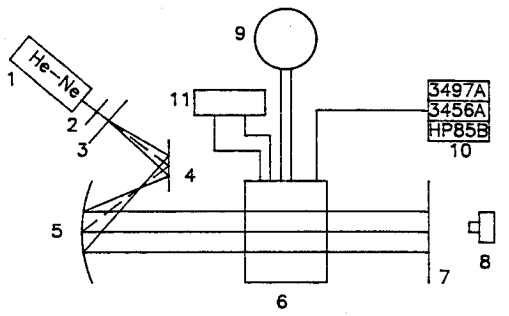

(1) laser, (2) pin hole, (3) condenser, (4) reflect mirror, (5) spherical mirror, (6) test section, (7) screen, (8) camera, (9) thermostat, (10) data acquisition system, (11) power supply.

Fig. 1 Schematic diagram of the experimental set-up.

(8). A highly sensitive thermostat (9) is used to supply water at constant temperature. By circulating water from the thermostat in the multipass countercurrent channel installed in the vertical and bottom walls of the rectangular cavity, the temperature of the vertical walls and the bottom walls of the rectangular cavity is kept constant. The wall temperature is measured by a calibrated thermocouple and recorded by using an HP-85B data acquisition system at (10). A special transparent coated electric heater is used to achieve contact melting at the beginning of the process. The heat will cause the separation of the solid PCM from the glass. Finally, this heater is connected to a power supply at section (11).

The experimental set-up is applied to the rectangular cavity with a cross section of 100 mm × 60 mm and a depth of 50 mm (Fig. 2). This test cell consists of the top cover (1), the auxiliary frame (2), the vertical cover (4), seat (6), and flanges (7) and (8), which are made of plexiglass. The vertical and horizontal heat exchangers (3) and (5) are made of copper in which the multipass countercurrent channel is machined. Furthermore, the surface of the heat source is grounded and polished to provide precise planar surfaces. Two layers of glass with 6 mm thickness at (9) are installed on each side of the test cell to form a window. This window allows optical and photographic observation of the melting zone. Therefore, the air gap between the two layers of glass is 10 mm thick. This is created to reduce the overall heat transfer coefficient between the test cell and the ambient. A special electric heater is formed by coating a layer of transparent electric conducting material on the glass. This heater is only used at the beginning of the experiment to separate the phase change material (PCM) from the glass. The temperature of the heat source at the surface is measured by calibrated copper-constentan thermocouples inserted beneath the surface about 1 mm deep. The solid-liquid interface location is determined photographically at different time intervals. Research grade *n*-heptadecane, $C_{17}H_{36}$, and *n*-eicosane, $C_{20}H_{42}$, are chosen as phase change materials. This is because their melting temperatures are close to ambient temperature and also are transparent in the liquid phase.

In the experiment, the solid-liquid interface position was determined photographically. The local Nusselt number on the vertical side walls during melting was determined by the shadowgraph technique. Different aspect ratios were obtained by filling the test cell with different liquid PCM levels. Since liquid paraffin possesses a high dissolving capacity for air, the phase material must be degassed carefully prior to each experiment. For this purpose, the PCM had undergone a solidification and melting cycle under vacuum, then it was carefully poured into the test cell, while its temperature was well above the melting point. To prevent the formation of internal voids, the solidification before melting was performed from bottom to top by cooling the bottom surface and maintaining the vertical side walls at a temperature slightly higher than the melting temperature of the phase change material used. When

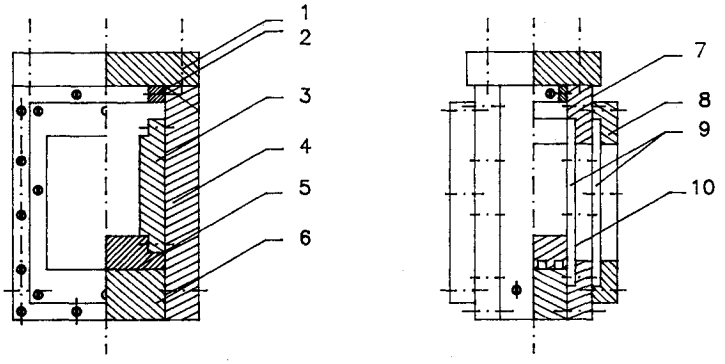

(1) top cover, (2) auxilary frame, (3) vertical heat exchanger, (4) vertical cover, (5) horizontal heat exchanger, (6) set, (7) flange, (8) flange, (9) glass window, (10) coated electrical heater.

Fig. 2 Schematic diagram of the test cell.

solidification was completed, the test material was heated to a desired uniform initial temperature. Later on, the coated electrical heater started to work, until melting near the glass plate occurred. Then, the experiment began by circulating water from a thermostat at the desired wall temperature.

Experimental Results

The important feature of contact melting is that the solid phase change material descends in the melting process by gravity. Six different solid-liquid interface shapes are shown in Fig. 3. Although each is taken at different time and different experimental parameters, as specified by the figure, they have common characteristics, e.g., the descending solid phase change material is almost in contact with the heat source surface at the bottom. A very thin melting layer, which could not be measured and could not be drawn in the above figure, formed between the solid and the bottom surface. The newly melted liquid is forced out of the channel and forced to flow to the top along the vertical walls. On the vertical walls, the thickness of the melting layer is almost uniform in height, in spite of having different time t, Stefan number Ste, subcooling parameter Sc, aspect ratio α^*, and phase change materials. At the top, the solid-liquid interface is very planar; therefore, except for the corners, the solid shape in the cavity is nearly rectangular.

The difference between contact melting and fixed melting in the rectangular cavity for the local Nusselt number on the vertical wall is shown in Figs. 4a and 4b. The local Nusselt numbers on the vertical wall are obtained by the shadowgraph technique.[25] The error associated with this type of experiment is estimated to be less than 15%.[26] Figure 4a is the typical result of a contact melting experiment. The parameters used in this experiment were $\alpha^* = 1.39$, $Ste = 0.0427$, $Sc = 0.0795$. The curves 1, 2, 3, . . . in Fig. 4a represent the instantaneous distribution of the local Nusselt number on the vertical wall at different time intervals. As can be seen, the local Nusselt number for different time intervals is uniform at first and then decreases with increasing height. The distance on which the Nusselt number remains constant is equal to the unmelted solid height in the rectangular cavity. At any time and height below the solid height, the local Nusselt numbers are uniform and have a maximum value, otherwise, they decrease. Figure 4b illustrates the typical results of fixed melting in the rectangular cavity. Fixed melting is completed by inserting a slender rod into the phase change material at the time of freezing and simultaneously fixing the end of the rod to the top of the rectangular cavity. This prevents the solid phase change material from dropping in the melting process. The fixed melting experimental parameters for Fig. 4b are $\alpha^* = 1.24$, $Ste = 0.0971$, $Sc = 0.0722$. As in Fig. 4a, the curves 1, 2, 3, . . . in Fig. 4b represent the instantaneous distribution

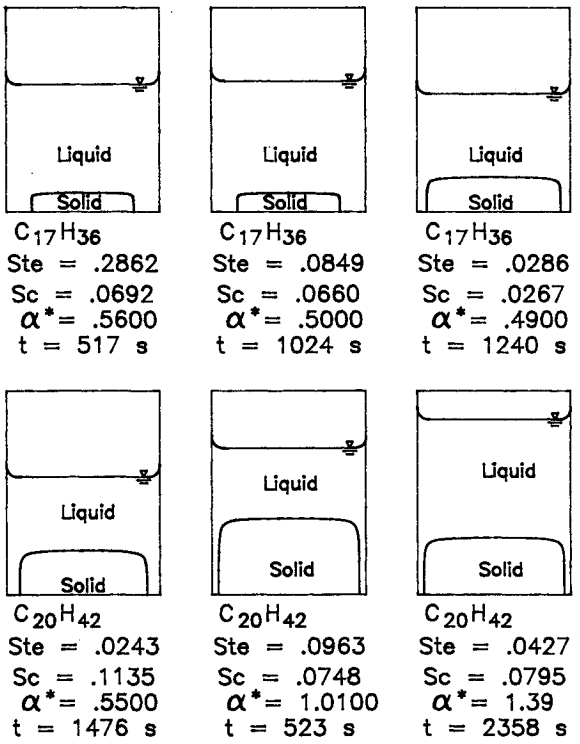

Fig. 3 Solid-liquid interface shape.

of the local Nusselt number on the vertical wall at different times. It must be noted that, as with PCM, n-eicosane is used in both contact melting and fixed melting for these two figures. Furthermore, it is seen from Fig. 4b that, in the initial period of fixed melting, the local Nusselt numbers do not change greatly in the height direction. However, as melting continues, the local Nusselt numbers decrease quickly with increasing height.

In comparing Figs. 4a and 4b, there is a significant difference between the instantaneous distribution of the local Nusselt number on the vertical wall for contact melting and for fixed melting. The shape of the solid-liquid interface for contact melting is nearly rectangular, whereas, for fixed melting, it is pear-like.[27] This is known as convection-controlled melting. Thus, it is inferred that conduction is the main mechanism of heat transfer in contact melting in the rectangular cavity.

Theoretical Modeling Analysis for Contact Melting

In order to observe the melting at the top of the solid, the following procedure is used. A very thin needle is solidified

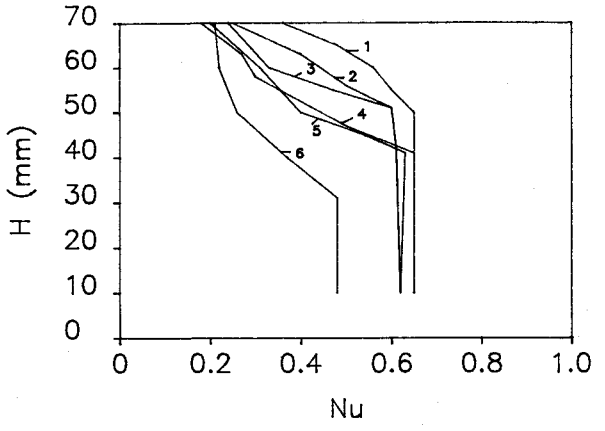

1. t = 762 (s) 2. t = 952 (s)
3. t = 1117 (s) 4. t = 1298 (s)
5. t = 1481 (s) 6. t = 1974 (s)

a) Contact melting

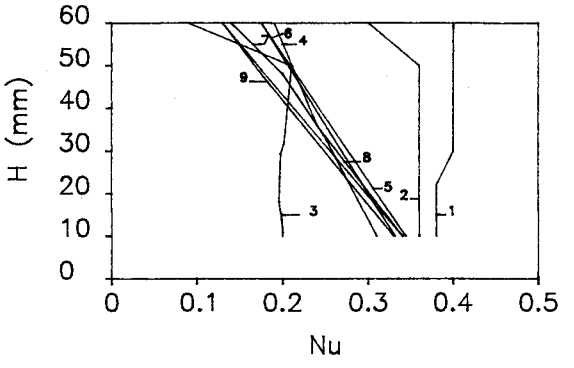

1. t = 356 (s) 2. t = 540 (s)
3. t = 691 (s) 4. t = 1405 (s)
5. t = 1843 (s) 6. t = 2222 (s)
7. t = 2861 (s) 8. t = 3535 (s)
9. t = 3915 (s)

b) Fixed melting

Fig. 4 Local Nusselt number on the vertical wall.

at the top of the solid PCM, and one of its ends is exposed beyond the top of the solid PCM. When contact melting is nearly finished, it is observed that the length of the exposed end of the needle has hardly increased and, thus, the solid liquid interface is maintained planar. This implies that less melting occurs at the top of the solid PCM. These experiments were conducted for several cases, and the same phenomenon occurred; therefore, in the following analysis, the melting at the top of the solid PCM is ignored.

A schematic of this model is shown in Fig. 5, along with two different coordinate systems. At time $t \geq 0$, the solid phase change material of height H_o in the rectangular cavity is at a uniform temperature $T_o < T_m$. As melting begins (at $t = 0$) and proceeds, the solid is assumed to descend vertically because of its own weight with a scale velocity of $\bar{U}(t)$. The melting layer thicknesses at the bottom and on the vertical walls are denoted by δ and δ_1, respectively. The rest of the variables are shown in Fig. 5, or in the Nomenclature. Mathematical descriptions are presented for three different regions: vertical melting region, bottom melting region, and solid region.

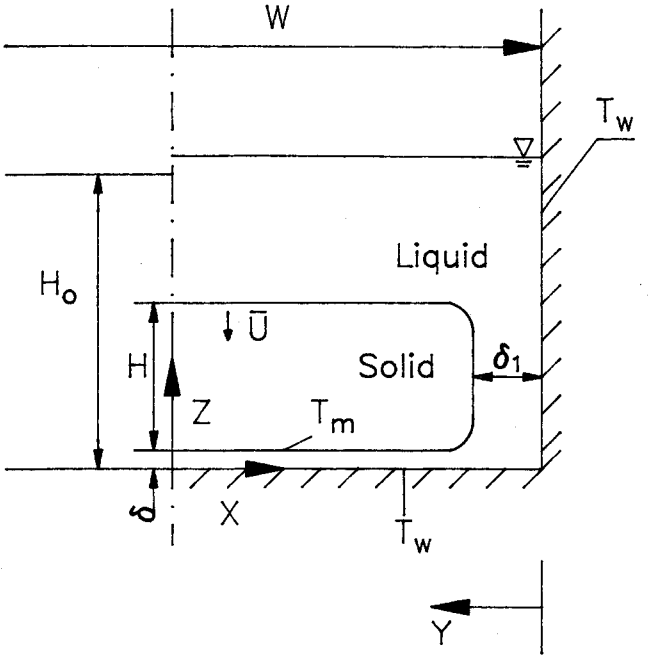

Fig. 5 Schematic diagram of the theoretical modeling.

Vertical Melting Region

As was mentioned earlier, conduction is the dominant mechanism of heat transfer. Thus, in this region, the one-dimensional melting equation is assumed to be

$$\frac{\partial T}{\partial t} = \alpha \frac{\partial^2 T}{\partial y^2} \tag{1}$$

with the following initial and boundary conditions of

$$\begin{aligned} @\ t = 0, &\quad T = T_o \\ @\ t > 0, &\quad y = 0 \quad \text{and} \quad T = T_w \\ @\ t > 0, &\quad y = \delta_1 \quad \text{and} \quad T = T_m \end{aligned} \tag{2}$$

Bottom Melting Region

In this region, the flow in the channel is considered as quasisteady and, also, natural convection is neglected. The channel is very thin, $\delta/W \ll 1$; therefore, the lubrication-approximation method used by other researchers is applied here. The inertia terms are negligible compared to the pressure gradient term, and also

$$\frac{\partial^2}{\partial x^2} \ll \frac{\partial^2}{\partial z^2} \tag{3}$$

Based on these assumptions, the governing equations in the bottom region are written as follows:

$$\text{Continuity:} \quad \frac{\partial u}{\partial x} + \frac{\partial v}{\partial z} = 0 \tag{4}$$

$$\text{Momentum:} \quad \mu \frac{\partial^2 u}{\partial z^2} - \frac{dp}{dx} \tag{5}$$

$$\text{Energy:} \quad u \frac{\partial T}{\partial x} + v \frac{\partial T}{\partial z} = \alpha \frac{\partial^2 T}{\partial z^2} \tag{6}$$

These equations are subjected to the following boundary conditions:

$$@\ z = 0, \quad u = v = 0 \quad \text{and} \quad T = T_w$$
$$@\ z = \delta(x, t), \quad u = 0, \quad v = -\bar{U}(t) \quad \text{and} \quad T = T_m \tag{7}$$

and $$z = \delta, \quad -k(1 + \delta'^2)\frac{\partial T}{\partial z} = \rho_\ell \bar{U} h_m^*$$

where $h_m^* = h_m + C_s(T_m - T_o)$ and $\delta' = \partial\delta/\partial x$. In addition, the subcooling of the solid phase change material is considered in the above equation.

Solid Region

For this region, the kinematic equation can be written as

$$\bar{U}(t) = -\frac{\partial H}{\partial t} - \frac{\partial \delta}{\partial t} \tag{8}$$

with the initial condition of

$$@\ t = 0, \quad H = H_o, \quad \text{and} \quad \delta = 0 \tag{9}$$

Also, the dynamic equation for this region can be written as

$$Mg - 2\int_0^{W/2-\delta_1} [P - P_{atm} - \rho_\ell g(H_o - H)\rho^*]\, dx = M\frac{d\bar{U}}{dt} \tag{10}$$

where

$$M = \rho_s H(W - 2\delta_1) \tag{11}$$

The method used by Moallemi[14] is extended here to solve the above combined equations. Accordingly, the dimensionless melting layer thickness on the vertical wall of the cavity is given by

$$\delta_1^* = 2\lambda(Fo)^{1/2} \tag{12}$$

where λ is determined by the equation,

$$\lambda \exp(\lambda^2) erf(\lambda) = Ste^*/(\pi)^{1/2} \tag{13}$$

The instantaneous dimensionless height of the solid phase change material is

$$H^* = \left\{\left(\frac{\alpha^*}{\rho^*}\right)^{3/4} - \frac{3}{4}[Ar\ Pr\ Ste^{*3}]^{1/4}\left[\frac{1}{6\lambda^2}(1 - (1 - 4\lambda Fo^{1/2})^{3/2}) - \frac{\sqrt{Fo}}{\lambda}\sqrt{(1 - 4\lambda\sqrt{Fo})}\right]\right\}^{4/3} \tag{14}$$

The dimensionless descending velocity of the solid phase change material can also be written as

$$\bar{U}^* = [Ar\ Pr\ Ste^{*3}\ H^*(1 - 4\lambda Fo^{1/2})^2]^{1/4} \tag{15}$$

The dimensionless melting layer thickness at the bottom is

$$\Delta = f(Ste^*)/\bar{U}^* \tag{16}$$

where

$$f(Ste^*) = \frac{1}{2}[(400 + 200\ Ste^* + 9\ Ste^{*2})^{1/2} - 3\ Ste^* - 20] \tag{17}$$

The melting rate is obtained as

$$V^* = 1 - \rho^* H^*(1 - \lambda Fo^{1/2})/\alpha^* \tag{18}$$

where V^* represents the melting rate, including the bottom and the two vertical walls. Inspection of Eq. (15) indicates that Δ is not a function of x. This has been verified through experimental observation. In this analysis, the width of cavity (W, distance between two vertical isothermal walls) is used as the characteristic length in the above equation.

Scale Analysis

It is difficult to clearly identify the functional dependency of the dimensionless parameters concerned with contact melting in a rectangular cavity. This leads to the question of what kind of function should be chosen as the basis for data reduction. In this paper, the scale analysis method is used to find the dependence relation among the parameters governing the contact melting in the rectangular cavity. Therefore, the experimental data can be reduced based on the results of the scale analysis. This method is a classical one, as described systematically by Bejan.[28] This scale method has been used to analyze the solid-liquid phase change problem since 1988. Jany and Bejan[29,30] analyzed the fixed melting in a rectangular cavity, with and without porous media, using the scale analysis method. Moutssoglou[31] presented the results of the scale analysis of solidification on the moving plate. The following scale analysis is applied in the case of contact melting in a rectangular cavity to find the functional dependence among the parameters. The scaling is performed on the model developed earlier, and executed as described by Bejan.[28] Physically, the following variables have the scale order of

$$x \sim (W - 2\delta_1), \quad z \sim \delta, \quad v \sim \bar{U}$$
$$\theta \sim (T_w - T_m), \quad y \sim \delta_1 \tag{19}$$

From Eq. (1), one can write

$$\frac{\theta}{t} \sim \frac{\alpha\theta}{\delta_1^2} \tag{20}$$

Therefore

$$\delta_1 \sim \sqrt{\alpha t} \tag{21}$$

Also, from Eq. (5)

$$u \sim \frac{P\delta^2}{\mu(W - 2\delta_1)} \tag{22}$$

and from Eq. (4)

$$\frac{u}{W - 2\delta_1} \sim \frac{v}{\delta} \sim \frac{\bar{U}}{\delta} \tag{23}$$

Upon substitution of Eq. (22) into Eq. (23), one obtains

$$P \sim \frac{\bar{U}}{\delta^3}\mu(W - 2\delta_1)^2 \tag{24}$$

and then by substitution of P into Eq. (21)

$$u \sim \frac{\bar{U}}{\delta}(W - 2\delta_1) \tag{25}$$

Assuming $d\delta/dx \ll 1$, from Eq. (7)

$$\frac{\theta}{\delta} \sim \frac{\rho_\ell \bar{U} h_m^*}{k} \tag{26}$$

and from Eq. (6)

$$\frac{u\theta}{W - 2\delta_1}, \qquad \frac{v\theta}{\delta} \sim \frac{\alpha\theta}{\delta^2} \tag{27}$$

Substituting Eqs. (25) and (26) into Eq. (27), it becomes

$$\frac{\bar{U}\theta}{\delta}, \qquad \frac{\bar{U}^2 h_m^*}{k} \sim \frac{\rho_\ell \bar{U} h_m^* \alpha}{k\delta} \tag{28}$$

from $\bar{U}\theta/\delta \sim \rho_\ell \bar{U}^2 h_m^*/k$, one obtains

$$\bar{U} \sim \frac{k\theta}{\delta \rho_\ell h_m^*} \tag{29}$$

In the melting process, the acceleration of the solid is much less than gravity acceleration g, and the term $d\bar{U}/dt$ in Eq. (10) is omitted. Basically, the scale order of Eq. (10) is as follows:

$$H(W - 2\delta_1)g(\rho_s - \rho_\ell) \sim P(W - 2\delta_1) \tag{30}$$

Combining Eq. (24) with Eq. (30), it follows that

$$Hg(\rho_s - \rho_\ell) \sim \mu \frac{\bar{U}}{\delta^3}(W - 2\delta_1)^2 \tag{31}$$

Substituting Eq. (29) into Eq. (31)

$$H \sim \frac{\bar{U}^4 (W - 2\delta_1)^2 (\rho_\ell h_m^*)^3 \mu}{g(\rho_s - \rho_\ell)\theta^3 k^3} \tag{32}$$

Since $\partial\delta/\partial t \ll dH/dt$, one can obtain $\bar{U} \sim H/t$ from Eq. (8) and substitute it into Eq. (32). Thus,

$$H^3 \sim \frac{t^4 g(\rho_s - \rho_\ell)\theta^3 k^3}{\mu(w - 2\delta_1)^2 (\rho_\ell h_m^*)^3} \tag{33}$$

Here, we choose $(W - 2\delta_1)$ as the characteristic length noted by $\bar{x}$, and so obtain the functional dependence between the dimensionless parameters. The final dimensionless forms of H^*, $\bar{U}^*\Delta$, δ_1^*, V^* are

$$H^* \sim (Ar\ Pr)^{1/3} Fo^{4/3}\ Ste^* \tag{34}$$

or

$$H^* \sim (Ar\ Pr)^{1/3} Fo^{4/3} \frac{Ste}{1 + Sc} \tag{35}$$

and

$$\bar{U}^* \sim \frac{Ste}{1 + Sc}(Ar\ Pr\ Fo)^{1/3} \tag{36}$$

$$\Delta \sim (Ar\ Pr\ Fo)^{1/3} \tag{37}$$

$$\delta_1^* \sim Fo^{1/2} \tag{38}$$

$$V^* \sim 1 - \frac{\rho^*}{\alpha^*}(Ar\ Pr)^{1/3} Fo^{4/3} \frac{Ste}{1 + Sc} \tag{39}$$

Although different characteristic lengths, W and $\bar{x}$ are used in the analytical solution and the scale analysis. This does not produce a severe difference in quality, because δ_1 is smaller in quantity.

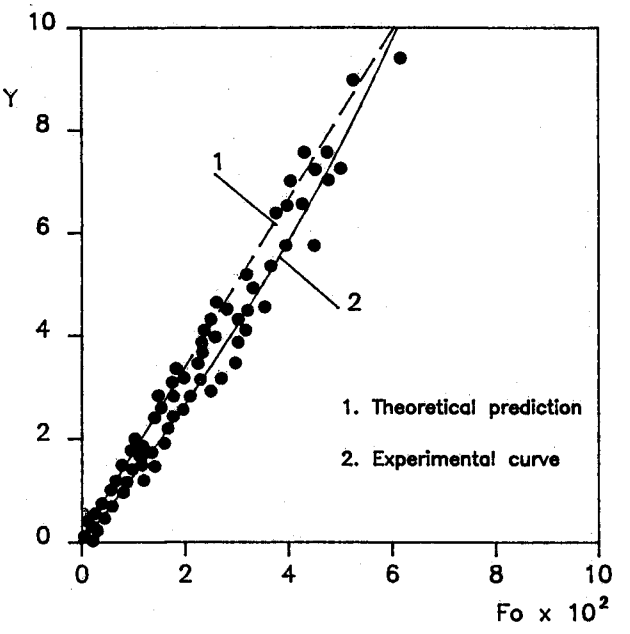

$$Y = 250\ V^*\ (\bar{x}/W)^{-11/3}\ (Ar\ Pr\ Ste^{*3})^{-1/3} \alpha^{*\,0.322}/\rho^*$$

Fig. 6 Comparison of melting rate data with theoretical modeling.

Comparison of Experimental and Analytical Results

The timewise variations of the melting rate are determined by measuring the area occupied by the solid and liquid phases, using the area meter with a precision of 0.1 mm². The uncertainty of the melting rate obtained by this measurement method is estimated to be less than 1%.[26] It must be noted that the melting rate includes all the melting in the rectangular cavity. The instantaneous solid height and some of the melting layer thickness on the vertical wall are also measured from the location of the solid-liquid interface. Based on the results of the scale analysis, the data for contact melting of *n*-eicosane in the rectangular cavity is reduced. Comparison of the contact melting rate data with theoretical prediction is given in Fig. 6. Curve 1 in this figure refers to the theoretical prediction of Eq. (18) and curve 2 is the experimental curve matching all the data, that is,

$$V^* = 0.8665\ \rho^*(\bar{x}/w)^{11/3} Ar^{-0.322}(Ar\ Pr\ Ste^{*3})^{1/3} Fo^{1.106} \tag{40}$$

The standard deviation associated with this equation is about 10.7%. The width of the cavity, the mean temperature of the wall, and the melting temperature are chosen as the characteristic dimension and the reference temperatures, respectively. Figure 7 is a comparison of the predicted dimensionless height of the solid with the experimental data for different experimental parameters. The solid line in Fig. 7 presents the theory of Eq. (14), corresponding to the experimental condition. It can be further seen that the maximum deviation between predicted and experimental data in Fig. 7 is about 17%. It is shown in Figs. 6 and 7 that the predicted values from the model agree well to some extent with the experimental data. There does exist some deviation, probably caused by measurement error and prediction model. In the model, the subcooling of the solid phase change material is considered in the modified latent heat, H_m^*, instead of in conduction. However, this is not valid for large Sc values. In this case, conduction in the solid should be taken into consideration. Also, melting at the top of the solid is not considered in the model, since melting it is small. This is another reason leading to the discrepancy between predicted values and experimental data.

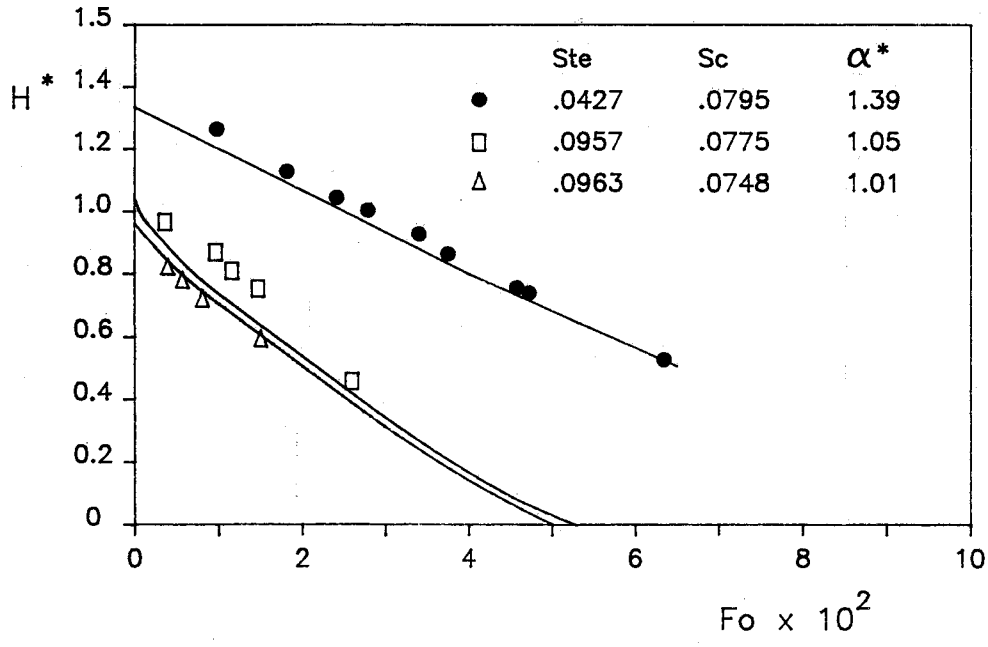

Fig. 7 Comparison of solid height data with theoretical modeling.

Conclusion

Contact melting experiments in a rectangular cavity are performed, and a predicted theoretical model is developed based on those experiments. The experimental data (e.g., the melting rate and the dimensionless height of the solid) are compared with predicted values of the theoretical model, and a good agreement is observed. From the analysis and observation of the melting phenomena, it is evident that the height of the microchannel at the bottom is constant. This demonstrates that heat transfer across the channel is dominated by conduction, although the melting liquid is still flowing in the channel. On the other hand, the melting layer thickness on the vertical wall is constant and the instantaneous local Nusselt number distribution is uniform below the height of the solid in the cavity. This indicates that the melting on the vertical wall is controlled by conduction. It is, therefore, concluded that heat conduction is the main mechanism of contact melting in a rectangular cavity.

The scale analysis is performed in order to find the functional dependence among the parameters of contact melting in the rectangular cavity. Hence, it is accurate to correlate the experimental data based only on the results of the scale analysis, and, thus, the scale analysis can provide the frame for data reduction.

Acknowledgment

The financial support provided partially by the Chinese National Science Foundation is greatly appreciated.

References

[1]Eckert, E. R. G., Goldstein, R. G., Pfender, E., Ibele, W. E., Patankar, S. W., Ramsey, S. W., Simon, T. W., Decker, N. A., Kuehn, T. H., Lee, H. O., and Girshick, S. L., "Heat Transfer—A Review of the 1985 Literature," *International Journal of Heat and Mass Transfer*, Vol. 29, No. 12, 1986, pp. 1767–1842.

[2]Eckert, E. R. G., Goldstein, R. G., Pfender, E., Ibele, W. E., Patankar, S. W., Ramsey, S. W., Simon, T. W., Decker, N. A., Kuehn, T. H., Lee, H. O., and Girshick, S. L., "Heat Transfer—A Review of the 1986 Literature," *International Journal of Heat and Mass Transfer*, Vol. 30, No. 12, 1987, pp. 2449–2523.

[3]Eckert, E. R. G., Goldstein, R. G., Pfender, E., Ibele, W. E., Patankar, S. W., Ramsey, S. W., Simon, T. W., Decker, N. A., Kuehn, T. H., Lee, H. O., and Girshick, S. L., "Heat Transfer—A Review of the 1987 Literature," *International Journal of Heat and Mass Transfer*, Vol. 31, No. 12, 1988, pp. 2401–2488.

[4]Kakac, S., Shah, R. K., and Aung, W., *Handbook of Single-Phase Convective Heat Transfer*, Wiley Interscience, NY, 1987.

[5]Shah, R. K., and London, A. L., *Laminar Flow Forced Convection in Ducts*, Academic, NY, 1978.

[6]Soloukhin, R. I., and Martyneko, O. G., "Heat and Mass Transfer Bibliography—Soviet Literature," *International Journal of Heat and Mass Transfer*, Vol. 26, No. 12, 1983, pp. 1771–1781.

[7]Martynenko, O. G., "Heat and Mass Transfer Bibliography—Soviet Literature," *International Journal of Heat and Mass Transfer*, Vol. 31, No. 12, 1988, pp. 2489–2503.

[8]Habib, I. S., and Dallman, R. J., "Heat Transfer with Phase Change," 1989 American Society of Mechanical Engineers/Winter Annual Meeting, Heat Transfer Division, 114, 1989.

[9]Viskanta, R., "Natural Convection in Melting and Solidification," *Natural Convection: Fundamentals and Applications*, edited by S. Kakac, W. Aung, R. Viskanta, Hemisphere, Washington, D.C., 1985, pp. 845–877.

[10]Viskanta, R., "Phase Change Heat Transfer," *Solar Heat and Storage: Latent Heat Materials*, edited by G. A. Lane, CRC Press, Baco Raton, FL, 1983, pp. 153–222.

[11]Emerman, S. H., and Turcotte, D. L., "Stokes' Problem with Melting," *International Journal of Heat and Mass Transfer*, Vol. 26, No. 11, 1983, pp. 1625–1630.

[12]Moallemi, M. K., and Viskanta, R., "Experiments on Fluid Flow Induced by Melting Around a Migrating Heat Source," *Journal of Fluid Mechanics*, Vol. 157, No. 1, 1985, pp. 35–71.

[13]Moallemi, M. K., and Viskanta, R., "Analysis of Close Contact Melting Heat Transfer," *International Journal of Heat and Mass Transfer*, Vol. 29, No. 6, 1986, pp. 855–867.

[14]Moallemi, M. K., Webb, B. W., and Viskanta, R., "An Experimental and Analytical Study of Close Contact Melting," *Journal of Heat Transfer*, Vol. 108, No. 4, 1986, pp. 894–899.

[15]Saito, A., Utata, Y., and Akiyoshi, M., "On the Contact Heat Transfer with Melting," (1st Report: Experimental Study), *Bulletin of Japanese Society of Mechanical Engineers*, Vol. 28, No. 240, 1985, pp. 1142–1149.

[16]Saito, A., Utata, Y., and Akiyoshi, M., "On the Contact Heat Transfer with Melting," (2nd Report: Analytical Study), *Bulletin of Japanese Society of Mechanical Engineers*, Vol. 28, No. 242, 1985, pp. 1703–1709.

[17]Saito, A., Utata, Y., and Yokihiro, Y., "Direct Contact Melting Heat Transfer on a Heated Surface," *Proceedings of 8th International Heat Transfer Conference*, San Francisco, CA, 1986, pp. 1805–1810.

[18]Saito, A., Utata, Y., and Yokihiro, Y., "On the Contact Heat Transfer with Melting," (3rd Report: The Melting on the Inner Surface of a Horizontal Cylindrical Tube), *Transaction of Japanese Society of Mechanical Engineers*, Vol. 53, No. 491, 1986, pp. 2130–2136.

[19]Bareiss, M., and Beer, H., "An Analytical Solution of the Heat Transfer Process During Melting of an Unfixed Solid Phase Change Material Inside a Horizontal Tube," *International Journal of Heat*

and Mass Transfer, Vol. 27, No. 5, 1984, pp. 739–746.

[20]Riviere, P. H., and Beer, H., "Experimental Investigation of Melting of Unfixed Ice in an Isothermal Horizontal Cylinder," *Int. Comm. of Heat Mass Transfer*, Vol. 14, No. 2, 1987, pp. 155–165.

[21]Sparrow, E. M., and Myrum, T. M., "Inclination-Induced Direct Contact Melting in a Circular Tube," *Journal of Heat Transfer*, Vol. 107, No. 3, 1985, pp. 533–540.

[22]Sparrow, E. M., and Geiger, G. T., "Melting in a Horizontal Tube with the Solid Either Constrained or Free to Fall Under Gravity," *International Journal of Heat and Mass Transfer*, Vol. 29, No. 7, 1986, pp. 1007–1019.

[23]Betzel, T., and Beer, H., "Solidification and Melting Heat Transfer to an Unfixed Phase Change Material Encapsulated in a Horizontal Concentric Annulus," *Wärme-und Stoffübertragung*, Vol. 22, No. 9, 1988, pp. 335–344.

[24]Dong, Z. F., "Research on Solid Liquid Phase Change Heat Transfer in a Rectangular Cavity with Phase Change Material-Contact Melting Study," Ph.D. Thesis, Xi'an Jiaotong Univ., Xian, China, 1988.

[25]Hauf, W., and Grigull, U., "Optical Method in Heat Transfer," *Advances in Heat Transfer*, Vol. 6, Academic, NY, 1970.

[26]Li, W. Y., "Heat Transfer and Interface Motion in the Presence of Subcooling for Melting Around a Horizontal Tube with and without Axial Fins," Master Thesis, Xi'an Jiaotong Univ., China, 1987.

[27]Ho, C. J., and Viskanta, R., "Experimental Study of Melting in a Rectangular Cavity," *Proceedings of ICHT*, 1982, pp. 369–374.

[28]Bejan, A., *Convection Heat Transfer*, Wiley Interscience, NY, 1984.

[29]Jany, P., and Bejan, A., "Scaling Theory of Melting with Natural Convection in an Enclosure," *International Journal of Heat and Mass Transfer*, Vol. 31, No. 6, 1988, pp. 1221–1235.

[30]Jany, P., and Bejan, A., "Scales of Melting in the Presence of Natural Convection in a Rectangular Cavity Filled with Porous Medium," *Journal of Heat Transfer*, Vol. 110, No. 2, 1988, pp. 526–529.

[31]Moutssoglou, A., "A Note on the Scale Analysis of Phase Change Problem," *Journal of Heat Transfer*, Vol. 110, No. 2, 1988, pp. 524–526.